Crystal Structures of RAE-1β and Its Complex with the Activating Immunoreceptor NKG2D

Pingwei Li, Gerry McDermott, and Roland K. Strong 13
Fred Hutchinson Cancer Research Center
Division of Basic Sciences
Seattle, Washington 98109
Lawrence Berkeley National Laboratory
Advanced Light Source
Berkeley, California 94720

Summary

Induced by retinoic acid and implicated in playing a role in development, rodent RAE-1 proteins are ligands for the activating immunoreceptor NKG2D, widely expressed on natural killer cells, T cells, and macrophages. RAE-1 proteins (α , β , γ , and δ) are distant major histocompatibility complex (MHC) class I homologs, comprising isolated $\alpha 1\alpha 2$ platform domains. The crystal structure of RAE-1 β was distorted from other MHC homologs and displayed noncanonical disulfide bonds. The loss of any remnant of a peptide binding groove was facilitated by the close approach of the groove-defining helices through a hydrophobic, leucine-rich interface. The RAE-1β-murine NKG2D complex structure resembled the human NKG2D-MICA receptor-ligand complex and further demonstrated the promiscuity of the NKG2D ligand binding site.

Introduction

Natural killer (NK) cells constitute an important component of innate immune system surveillance against tumor cells and cells infected by viruses or intracellular pathogens (Trinchieri, 1989). NK cells regulate innate and acquired immune responses through the release of various immune modulators, such as interferon-γ, or by directly destroying compromised cells. NK cell surface receptors (NCRs) belong to either of two families defined on the basis of structural homologies. The first family consists of type I transmembrane glycoproteins containing one to three tandem immunoglobulin-like domains in the ectodomain; the second comprises homoand heterodimeric type II transmembrane glycoproteins containing C-type lectin-like NK receptor domains (NKDs) (Weis et al., 1998). Many NCRs in both families are specific for classical and nonclassical MHC class I proteins and occur in paired activating and inhibitory isoforms (Bakker et al., 2000). Different NCRs, with different MHC class I specificities, are expressed on overlapping subsets of NK cells. Thus, NK cell effector functions are regulated by integrating signals across the array of stimulatory and inhibitory NCRs engaged upon interaction with target cell surface NCR ligands, resulting in the elimination of cells with reduced MHC class I expression (Lanier, 2000).

NKG2D is an activating, NKD-type immunoreceptor whose expression was first recognized on NK cells but

was subsequently found on CD8 $^+$ $\alpha\beta$ T cells, $\gamma\delta$ T cells, and macrophages, making it one of the most widely distributed immunoreceptors currently described (Bauer et al., 1999; Wu et al., 1999). Despite inclusion in the NKG2 family, NKG2D displays only limited sequence similarity to other NKG2 NCRs or CD94 (20%–30% identical) and forms homodimers rather than NKG2/CD94 heterodimers. NKG2D engagement is signaled by recruitment of phosphatidylinositol 3-kinase through the adaptor molecule DAP10 (Wu et al., 1999, 2000), whereas other activating NCRs utilize the DAP12 adaptor molecule (Lanier et al., 1998).

In humans, NKG2D ligands include the closely related cell surface proteins MICA and MICB (Bahram et al., 1994; Bahram and Spies, 1996; Groh et al., 1996) and the human cytomegalovirus UL16 binding proteins known as ULBPs (Cosman et al., 2001), all distant MHC class I homologs that do not function in conventional antigen presentation. NKG2D-MIC recognition events stimulate effector responses from NK cells and $\gamma\delta$ T cells and may positively modulate CD8⁺ $\alpha\beta$ T cell responses, thus serving a costimulatory function (Bauer et al., 1999; Groh et al., 1998). On macrophages, stimulation through NKG2D triggers TNF α production and release of nitric oxide (Diefenbach et al., 2000). Unlike other immunoreceptor ligands, which include constitutively expressed classical and nonclassical MHC class I proteins, the NKG2D ligands MICA and MICB are induced by cellular stress (Groh et al., 1996, 1998) and have a tissue distribution largely restricted to the intestinal epithelium and epithelially derived tumors (Groh et al., 1996, 1999). The recent crystal structure of the MICA-NKG2D complex revealed an NKG2D homodimer bound to a MICA monomer in an interaction analogous to $\alpha\beta$ T cell receptor-MHC class I protein complexes. This was also argued to be useful for modeling the salient details of the NKG2A-CD94-HLA-E interaction (Li et al., 2001), but was quite unlike either of the interactions observed in the crystal structure of the complex between the murine NKD-type NCR Ly49A and its MHC class I ligand H-2Dd (Tormo et al., 1999). ULBPs are homologous to the $\alpha 1\alpha 2$ peptide binding platform domains of MHC class I proteins, but lack α 3 domains and are anchored in the membrane by GPI linkages.

Murine and human NKG2D (huNKG2D) ectodomains are 69% identical. While rodents lack any recognizable homologs of MICA and MICB, murine NKG2D (muNKG2D) ligands include the retinoic acid-inducible RAE-1 family of proteins and the H60 minor histocompatibility antigen (Cerwenka et al., 2000; Diefenbach et al., 2000). Like the ULBPs, RAE-1 and H60 are homologous to the platform domains of MHC class I proteins, lack α 3 domains, and are also anchored in the membrane by GPI linkages. The RAE-1 family, first identified as cDNAs induced in response to retinoic acid treatment of a murine carcinoma cell line (Zou et al., 1996), comprises four highly homologous isoforms (≥92% identical), RAE-1 α , β , γ , and δ , which are highly expressed during embryonic development (particularly in the brain) but are rare in normal adult tissues (Cerwenka et al.,

³ Correspondence: rstrong@fhcrc.org

2000; Diefenbach et al., 2000; Nomura et al., 1994, 1996). It has recently been shown that tumors expressing RAE-1 molecules can be recognized by NK cells and rejected (Diefenbach et al., 2001). Like NKG2D-MIC stimulation of NK cells, RAE-1-mediated rejection can override inhibitory signals from the expression of self MHC class I proteins on the tumor cells.

H60 was originally identified as an immunodominant minor histocompatibility antigen, acting through the H-2Kb-restricted presentation of an H60-derived peptide (Malarkannan et al., 1998, 2000). Though differentially expressed in inbred mouse strains, H60 transcripts were found at low levels in embryonic tissue and at significant levels on macrophages and dendritic cells in the spleen (Malarkannan et al., 2000). In solution, muNKG2D binds more tightly to RAE-1 ($K_D = 486$ nM) and H60 ($K_D =$ 18.9 nM) than most cell surface immunoreceptor-ligand interactions (O'Callaghan et al., 2001), though the strength of the muNKG2D-RAE-1 interaction is on the order of the huNKG2D-MICA interaction ($K_D = 1 \mu M$) (Li et al., 2001). Both ligands compete directly for NKG2D, though the muNKG2D-H60 interaction makes greater use of electrostatic interactions (O'Callaghan et al., 2001). Neither interaction is affected by the glycosylation state of any of the molecules (O'Callaghan et al., 2001).

We report here the 2.85 Å resolution crystal structure of RAE-1 β and a model of the RAE-1 β -muNKG2D complex based on 3.5 Å resolution diffraction data to further characterize the structural basis for ligand recognition by NKG2D. The RAE-1 β crystallographic analysis revealed a very distorted MHC class I platform structure. Despite little recognizable structural similarity between RAE-1 β and MICA beyond retention of the underlying MHC class I platform fold, the modeled complex revealed that muNKG2D and RAE-1 β interact in a manner very similar to huNKG2D and MICA.

Results

Molecules like H-60 and RAE-1 represent the distillation of the MHC class I fold down to what is likely to be its minimal folding unit: an isolated $\alpha 1\alpha 2$ platform domain. In order to study this variation of the MHC class I fold, we determined the crystal structure of RAE-1ß (residues 1-178) at 2.85 Å resolution by multiple isomorphous replacement (MIR), taking advantage of 5-fold noncrystallographic symmetry in the crystals (Table 1). The activating immunoreceptor NKG2D displays the ability to recognize a variety of polymorphic and nonpolymorphic ligands in the human immune system. To examine the extent to which this plasticity of recognition extends to the highly conserved muNKG2D protein, we modeled the RAE-1β-muNKG2D complex using 3.5 Å resolution diffraction data collected from crystals grown with bacterially expressed recombinant protein refolded from inclusion bodies. The structure of the RAE-1 β muNKG2D complex was determined by molecular replacement (MR) using the refined crystal structures of RAE-1β and muNKG2D (Wolan et al., 2001) as search models (Table 1).

RAE-1ß Structure

The fold of RAE-1 β was clearly homologous to the $\alpha 1\alpha 2$ platform domains of MHC class I molecules, as pre-

dicted (Zou et al., 1996), with two long, interrupted, roughly parallel α helices arranged on an eight-stranded antiparallel β sheet (Figure 1). These α helices define the groove in which ligand, peptide or otherwise, binds in MHC class I proteins and homologs that bind a ligand (Figure 2). The structure of the β sheet in RAE-1 β was fairly well conserved when compared with the structures of MICA (Li et al., 1999, 2001) (root mean square deviation [rmsd] of 0.97 Å between 46 pairs of $C\alpha$ atoms) or classical MHC class I molecules (rmsd of 1.16 Å between 51 pairs of Cαs using H-2Dd as a representative structure; Figure 2). However, the two α helices in RAE-1 β were positioned much closer to each other than in any other MHC class I protein or homolog, close enough to be covalently linked through a noncanonical disulfide bond (between Cys60 and Cys160; Figures 1B and 1C). The distances between $C\alpha$ atoms lining the interior of the groove were from 5.3 to 7.5 Å, while the distances between the analogous $C\alpha$ positions in conventional, peptide binding MHC class I molecules ranged from 13 to 14 Å, resulting in the loss of any recognizable remnant of a ligand binding pocket in RAE-1β (Figures 1B and 3). Closing the groove was accomplished by inward movements of the helical elements in both the α 1 and α 2 domains toward each other, yielding a platform domain structure that was the most dramatically rearranged from classical class I protein structures of any MHC class I homolog so far reported (Figure 2 and Table 2). The close approach of the helices was sealed by the noncanonical disulfide bond and an unprecedented hydrophobic interhelical interface consisting of residues Val57, Leu61, Pro64, Leu65, Leu68, Leu72, Val81, Ile139, Trp143, Phe149, Leu156, Met164, Phe167, Leu168, and the aliphatic portions of the side chains of Lys71, Lys75, and Lys163 (Figure 1B). Despite the preponderance of leucine residues at this interface, the interaction between helices was unlike canonical leucine zipper packings. Additional interhelical interactions occurred between residues on the exposed surface of RAE-1 β : Asp146 made ionic interactions with Lys71 and Lys75; Gln152 hydrogen bonded to the peptide backbone of Leu68; and Glu170 hydrogen bonded with Asn53 and Ser51.

The asymmetric unit of the RAE-1ß crystals provides five separate views of the structure (Figure 2A). The largest differences among these models occurred in loops arranged around the edges of the platform domain. The loop between Gln100 and Thr105 (β 1 β 2 in the α2 domain) adopted two different conformations, one observed in three RAE-1 β molecules and another in the other two, due to different interactions with neighboring molecules in the crystal. The α 1 domain β 4 α 1 (Lys44-Glu53) and interdomain α 2 β 1 (Val79–Gly90) loops were poorly defined in the electron density maps and exhibited the largest B factors seen in the structure (exceeding 150 Å² for some side chains) and the largest rmsds between molecules. This suggests that these loops are flexible, as is also the case in the MICA structure (Li et al., 1999). However, interpretable electron density is present for these residues, and their presence in the model improves the Rfree (Brünger, 1992). The core region of RAE-1β, excluding the flexible loops but including all the defined secondary structure elements, was very conserved, with rmsds between the five RAE-1 β molecules of only 0.56-0.75 Å (144 pairs of C α s).

Table 1. Data Collection and Refin	ement Statistics				
Data Collection and Phasing Data Set	RAE-1β	RAE-1β/Hg1	RAE-1β/Hg2	RAE-1β/Au	RAE-1β-NKG2D
Condition	Native	Hg (CN) ₂	K₂HgI₄	NaAuCl₄	Native
Number of sites	-	5	5	6	-
Wavelength (Å)	1.1000	Cu Kα	Cu Kα	Cu Kα	0.9793
Resolution (Å)	2.85	4.00	4.00	4.00	3.50
Highest shell (Å)	2.90-2.85	4.07-4.00	4.07-4.00	4.07-4.00	3.58-3.50
Unique reflections	38,675	13,783	13,398	12,422	8417
Redundancy	10.4	4.89	6.01	5.01	3.48
Completeness (%)	100.0 (100.0)	97.0 (97.4)	94.6 (94.4)	88.7 (91.2)	99.3 (100.0)
< I/σ(I)>	37.5 (3.8)	9.1 (3.2)	12.2 (5.3)	14.7 (3.1)	8.4 (3.2)
R _{sym} (%)	7.90 (46.0)	15.0 (38.2)	15.1 (32.1)	11.9 (39.8)	10.1 (22.9)
R _{iso} (%)	_	23.0	20.9	19.8	=
R _{cullis} (%; centrics/acentrics)		0.64/0.63	0.64/0.67	0.96/0.96	-
Phasing power (centrics/acentrics))	1.92/1.47	1.96/1.32	0.64/0.67	-
Overall figure-of-merit	52%				
(15–4.00 Å):					
Refinement of:	RAE-1β	Complex			
Resolution (Å)	25-2.85	20-3.50			
Reflections (all F >0;	34,652/2839	8115/1373			
working/test)					
Protein / solvent atoms	7025/42	3383/0			
R _{crvst} / R _{free} (%)	23.4/27.9	31.4/33.0			
Average Group B-factor (Ų)	89.0	53.4			
Wilson intercept (Ų)	88.9	58.7			
Cross validated σ _A	0.68	0.69			
coordinate error (Å)					
Geometry (rmsd from ideality)					
Bond length (Å)	0.010	0.017			
Bond angles (°)	2.0	2.0			
Ramachandran					
Most favored (%)	78.5	82.3			
` ,		15.3			
Additional allowed (%)	16.9	10.0			
Additional allowed (%) Generously allowed (%)	16.9 4.5	1.3			

Values for the highest resolution shell are shown in parentheses. $R_{\text{sym}} = \Sigma |I - <I>|/\Sigma <I>$ where I is the observed intensity, <I> is the mean intensity of multiple observations of symmetry-related reflections. $R_{\text{cullis}} = \Sigma |F_{\text{PH}} - F_{\text{P}}| - |F_{\text{Hcalc}}|/\Sigma |F_{\text{PH}} - F_{\text{P}}|$ where F_{P} is the protein structure factor amplitude and F_{PH} is the heavy atom derivative structure factor amplitude phasing power = $<|F_{\text{H}}|>/E$ where F_{H} is the heavy atom structure factor amplitude and E is the residual lack-of-closure error. R_{cryst} , $R_{\text{free}} = \Sigma ||F_{\text{obs}}| - |F_{\text{calc}}||/\Sigma ||F_{\text{obs}}|$ where F_{obs} and F_{calc} are the observed and calculated structure factor amplitudes. R_{free} is calculated from randomly chosen reflections excluded from refinement (Brünger, 1992). Geometry was analyzed with PROCHECK (Laskowski et al., 1992); note that the quality of the complex structure to a large extent reflects the input search models, since this structure is only partially refined.

When all common $C\alpha s$ are considered (174), rmsds for pairwise superpositions range from 1.96 to 2.37 Å; excluding the two flexible loops (accounting for 22 $C\alpha s$) improves the rmsds to between 1.12 and 2.03 Å.

MHC class I molecules display two "high points" on the helix side of the platform domain formed at bends (at Glu58 and Ala150 in H-2D) in the groove-defining α helices. These features restrict the orientation of TCRs in MHC-TCR complexes (Wilson and Garcia, 1997) and NKG2D in the MICA-huNKG2D complex (Li et al., 2001). RAE-1 β retained a similar feature in the α 2 domain, between helices H1 and H2a (at Gly147), but lacked any comparable feature in the $\alpha 1$ domain. Helix 2b in the $\alpha 2$ domain was considerably further away from the β sheet and moved by about 5 Å toward helix H1 in the α 1 domain compared with the corresponding segment of helix (Arg151-Gly162) in H-2Dd or other MHC class I proteins. The formation of the disulfide bond between the helices also coincided with two bends of approximately 44° and 47° at Leu61 within α 1 domain helix H2 and at Ser161 between α 2 domain helices H2a and H2b, where corresponding regions in class I molecules are continuously helical.

There were two disulfide bonds in RAE-1 β , neither of which is conserved in related structures. One cysteine (Cys160) in the disulfide bond that connected the two helices in RAE-1 β (Cys60-Cys160) was conserved in all MHC class I protein and homolog structures, where it, rather, participates in a disulfide bond with a cysteine (Cys96 in MICA and Cys101 in H-2Dd) in the β 1 strand of the α 2 domain. The second disulfide bond (Cys7-Cys26) connected strands β 1 and β 2 in the α 1 domain. ULBPs (Cosman et al., 2001) retain the canonical cysteine arrangement, while the cysteines in H60 are arranged differently from either RAE-1 or MHC class I proteins.

Structure of the RAE-1β-NKG2D Complex

MuNKG2D bound diagonally across the top of RAE-1 β , straddling the two helices, in a manner analogous to the interaction between huNKG2D and MICA (Li et al., 2001) (Figure 3), but quite unlike that of other immunoreceptor-

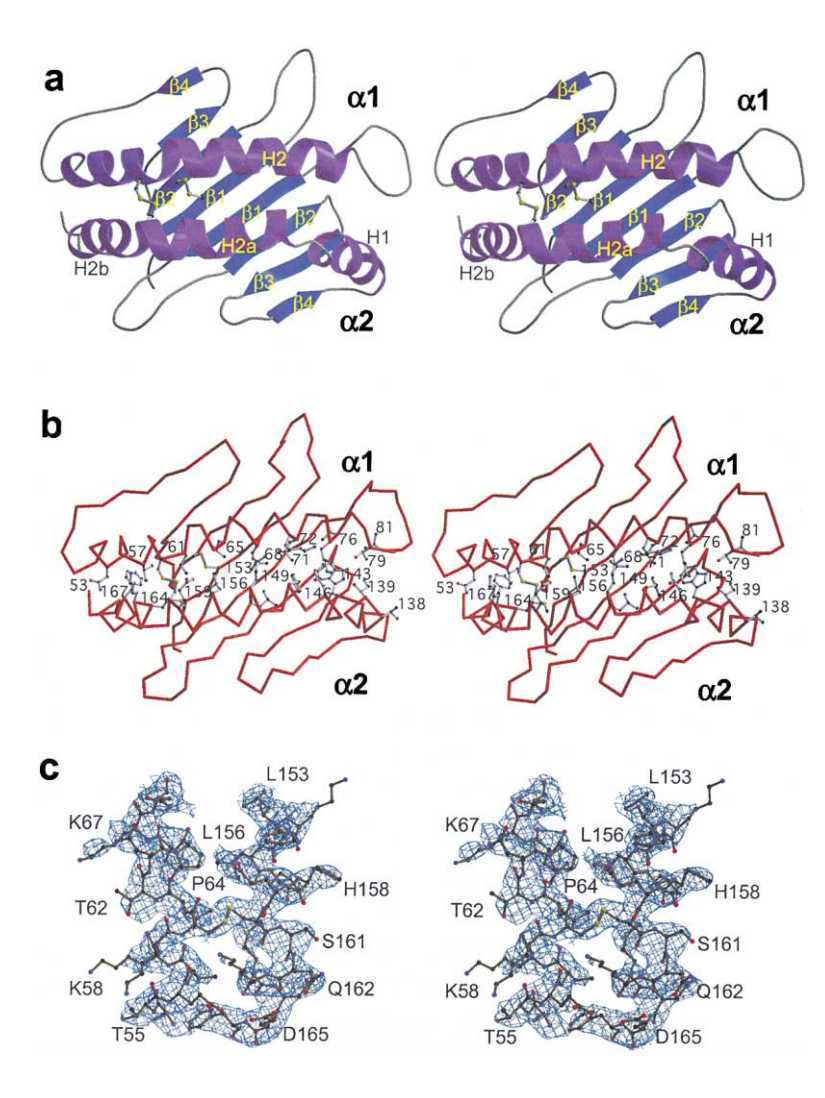


Figure 1. Structure of RAE-1β

Stereo views are shown of (A) a ribbon representation of the structure of RAE-1 β . (B) a C α backbone representation of the structure of RAE-1B highlighting residues lining the interhelical surface, and (C) the experimental electron density map (after NCS averaging) around the noncanonical disulfide bond between Cys60 and Cys160 contoured at $1\sigma.$ In (A), secondary structure elements have been assigned using standard MHC class I nomenclature; α helices are shown as purple corkscrews, β strands as blue arrows, and coil as gray tubes; disulfide bonds are shown in balland-stick mode. In (B), side chains are shown for residues (left to right) Asn53, Val57, Cys60, Leu61, Leu65, Leu68, Lys71, Leu72, Lys75, Val76. Thr79, and Val81 in the α1 domain helix and (right to left) Val138, Ile139, Trp143, Asp146, Phe149, Gln152, Leu153, Leu156, Glu159, Cys160, Lys163, Met164, and Phe167 in the $\alpha 2$ domain helices; for clarity, not all residues have been labeled. Figures were generated with MolScript (Esnouf, 1999) and Raster3D (Merrit and Bacon, 1997).

ligand complex crystal structures. The orientation of muNKG2D relative to the RAE-1β platform was slightly different from MICA-NKG2D complex; when murine and huNKG2D in the two complexes were superimposed, RAE-1 β was displaced from the position of the MICA platform domain by a rotation of 20°-25° and a translation of approximately 7 Å, moving the C terminus of RAE- 1β into the body of the superimposed MICA platform (Figures 2C and 2D). The effect of this relative movement in the complexes was to bring certain ligand structural elements closer into alignment, such as the α 2 domain H2a and H2b helices that provide multiple contacts to NKG2D-B, while moving many other elements apart. such as the $\alpha 1$ domain H2 helix and the H1 helix in the α 2 domain (Figures 2C and 2D). The MICA platform loop that deviated most dramatically from canonical MHC class I structures, the $\alpha 1$ domain $\beta 1\beta 2$ loop, provided several key NKG2D-A $\beta5'\beta5$ "stirrup" loop contacts in the MICA-huNKG2D complex. This loop in RAE-1 β (residues 13-20) was much more similar to canonical structures but, due to the reorientation of the ligand in the NKG2D binding saddle, comparably provided several contacts to the muNKG2D-A stirrup loop (Figure 2D and Table 3).

Unlike the MICA-huNKG2D interaction, where signifi-

cant conformational changes occurred in MICA upon binding (Li et al., 2001), no large changes occurred in the backbone structures of muNKG2D or RAE-1 β after complex formation. Rmsds for the superpositions of muNKG2D in the complex and the search model (1HQ8.pdb) were 0.24 Å or 0.49 Å (per monomer) on all 123 C α s and for RAE-1 β alone or in the complex were 0.36 Å on all 174 C α s. The only observed movements required to prevent steric clashes in the complex involved the side chains of His58, Gln70, Glu148, and Phe155 in RAE-1β. Monomer A of muNKG2D (muNKG2D-A) interacted mostly with the C-terminal segment of helix H2 and a few residues at the β 1 β 2 loop in the α 1 domain of RAE-1ß, while muNKG2D monomer B (muNKG2D-B) interacted predominantly with helix H2b in the α 2 domain (Table 3).

The total buried solvent-accessible surface area at the muNKG2D-RAE-1 β interface was roughly 1700 Ų, which was comparable to most TCR-MHC class I interfaces (1700–1800 Ų), but smaller than the surface area buried at the MICA-NKG2D interface (2200 Ų) (Li et al., 2001). Like the MICA-huNKG2D complex, the contribution to the interaction was fairly evenly split between the two halves of the muNKG2D homodimer, with 874 Ų buried at the muNKG2D-A-RAE-1 β α 1 domain interface

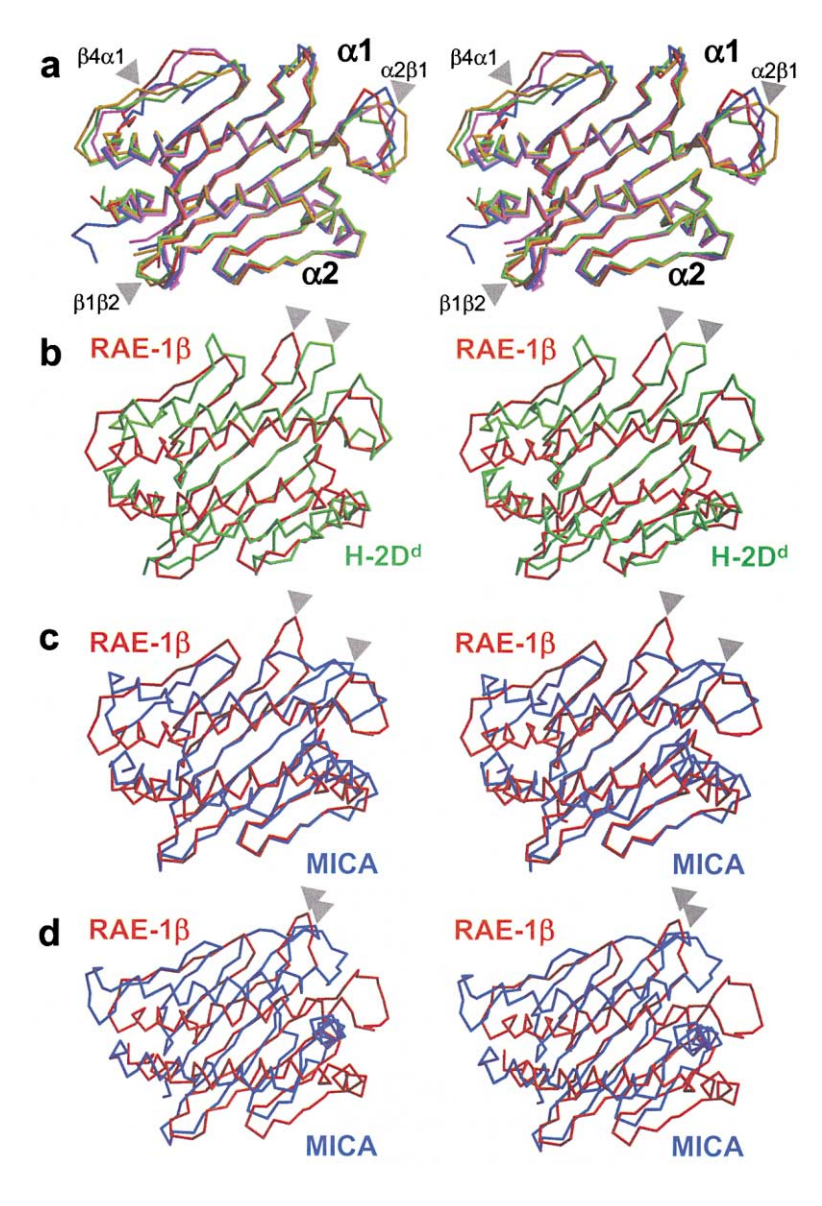


Figure 2. Comparisons of RAE-1 β with the Platform Domains of MHC Class I Molecules and Human MICA

Stereo views are shown of $C\alpha$ backbone representations of (A) the superposition of the five RAE-1β molecules in the asymmetric unit; (B) the superposition of RAE-1 β (red) on the platform domain of H-2Dd (green); and (C and D) the superposition of RAE-1β (red) on the platform domain of MICA (blue). In (B) and (C), the superposition was based on structurally conserved $C\alpha$ atoms in the platform domain $\boldsymbol{\beta}$ sheet. In (D), the superposition was based on the alignment of muNKG2D and huNKG2D in the two complexes, thus highlighting the relative repositioning of the ligand between the two complexes. In (A), the five structures are colored differently, and loops discussed in the text are labeled; in (B-D), arrows indicate analogous points in the \$1\$2 loops in the α 1 domains.

and 794 Ų buried at the muNKG2D-B-RAE-1 β α 2 domain interface. The close approach of the two RAE-1β helices apparently contributed to the reduction of the total solvent accessible surface area buried in the muNKG2D-RAE-1β complex by reducing the quality of the fit of RAE-1ß onto muNKG2D relative to the fit between MICA and the analogous surface of huNKG2D. Using the calculated shape correlation statistic (Sc) (Lawrence and Colman, 1993), a measure of the degree that two contacting surfaces are a geometric match, the muNKG2D-RAE-1β complex yielded an Sc value of 0.63 (where 1.0 represents a theoretically perfect match), whereas the MICA-NKG2D interface yields an Sc of 0.72. However, the complementarity of the muNKG2D-RAE- 1β interface was comparable to the high end of the interactions between TCRs and MHC class I proteins, where Sc values range from 0.46 to 0.63.

Most of the residues involved in the interaction between RAE-1 β and muNKG2D were either polar or charged residues (about 38% and 42%, respectively, out of a total of 21 contact residues) (Table 3), consistent

with an interface dominated by hydrogen bonds and salt bridges. The resolution of the complex crystallographic analysis limited the detail that these interactions could be delimited. However, three pairs of residues, Lys166 (muNKG2D-B) and Glu148 (RAE-1ß), Lys213 (muNKG2D-B) and Glu159 (RAE-1B), and Glu217 (muNKG2D-B) and Lys151 (RAE-1β), appeared to form good candidate salt bridges. In contrast, the muNKG2D-A-RAE-18 half-site showed poorer charge complementarity, with interactions between these two molecules dominated by potential hydrogen bonding and hydrophobic interactions (Figure 3A and Table 3). Like the MICA-huNKG2D complex, the RAE-1β contact surfaces on muNKG2D were clustered around two conserved tyrosine residues, Tyr168 and Tyr215, on both muNKG2D-A and -B. Although most of the residues interacting with RAE-1β are conserved in both murine and human NKG2D, they interacted with a different set of ligand residues in different ways than in the MICAhuNKG2D complex (Li et al., 2001) (Table 3). Though involving fewer residues than in the MICA-huNKG2D

Table 2. Movements of Helical Elements in MHC Class I Homologs Relative to Classical Class I Proteins

Molecule	Reference	Rmsd (Å)	α1: H2 (Å)	α 2: H1 (Å)	α 2: H2a (Å)	α 2: H2b (Å)
HFE	Lebrón et al. (1998)	0.72	3.5–3.8	<1	~	~
ZAG	Sanchez et al. (1999)	0.79	<1	2.7	<1*	\sim
H-2T22	Wingren et al. (2000)	0.93	1.5 (C)-5.8 (N)	absent	absent	1.8-2.2
MICA	Li et al. (1999)	1.16	2.4-2.7	8.8 (C)	\sim	\sim
CD1	Zeng et al. (1997)	1.21	<1-7.5 (N)	2.5-3.0	4.6 (N)	\sim
FcRn	Burmeister et al. (1994)	1.43	4.0 (N)/6.2* (C)	4.1-8.3	5.0 (N)	4.0 (C)
RAE-1β	(this report)	1.82	<1-7.8 (N)	5.6 (C)	4.6-7.4	2.5 (N) / 4.8* (C)

MHC class I homologs, ranked above by rmsd score, were aligned on the highly conserved six-strand core of the antiparallel β sheet in the platform domain, except for H-2T22, where only five strands are well conserved. All comparisons were made against the murine MHC class I protein H-2D^d (Tormo et al., 1999). Movements of the four separate helical elements that define the peptide-binding groove (H2 in the α 1 domain and H1, H2a, and H2b in the α 2 domain) relative to their position in H-2D^d are shown. Only movements towards (or away from, indicated with an asterisk) where the peptide groove would lie are shown. Movements of the ends of the helical elements are indicated [(N), N terminus; (C), C terminus] if one end of the helical element dominates the relative movement. Tildes indicate little significant movement. HFE refers to the human hemochromatosis associated protein; ZAG is human Zn- α_2 -glycoprotein; H-2T22 is a murine $\gamma\delta$ TCR ligand; FcRn refers to the rat neonatal Fc receptor.

complex, the muNKG2D-RAE-1 β interaction was similar in that the RAE-1 β contacting surfaces on NKG2D-A and -B have in common a core set of residues that make very distinct interactions on either domain of RAE-1 β (Table 3).

In the crystals, muNKG2D-RAE-1ß complexes inter-

acted with each other along a crystallographic 6_1 screw axis (Figure 4), making reciprocal, predominately hydrophobic contacts through residues in the otherwise flexible $\beta 3\beta 4$ loop (residues 174–178) of muNKG2D (secondary structure elements in muNKG2D have been labeled as in Li et al. (2001) and Wolan et al. (2001). The

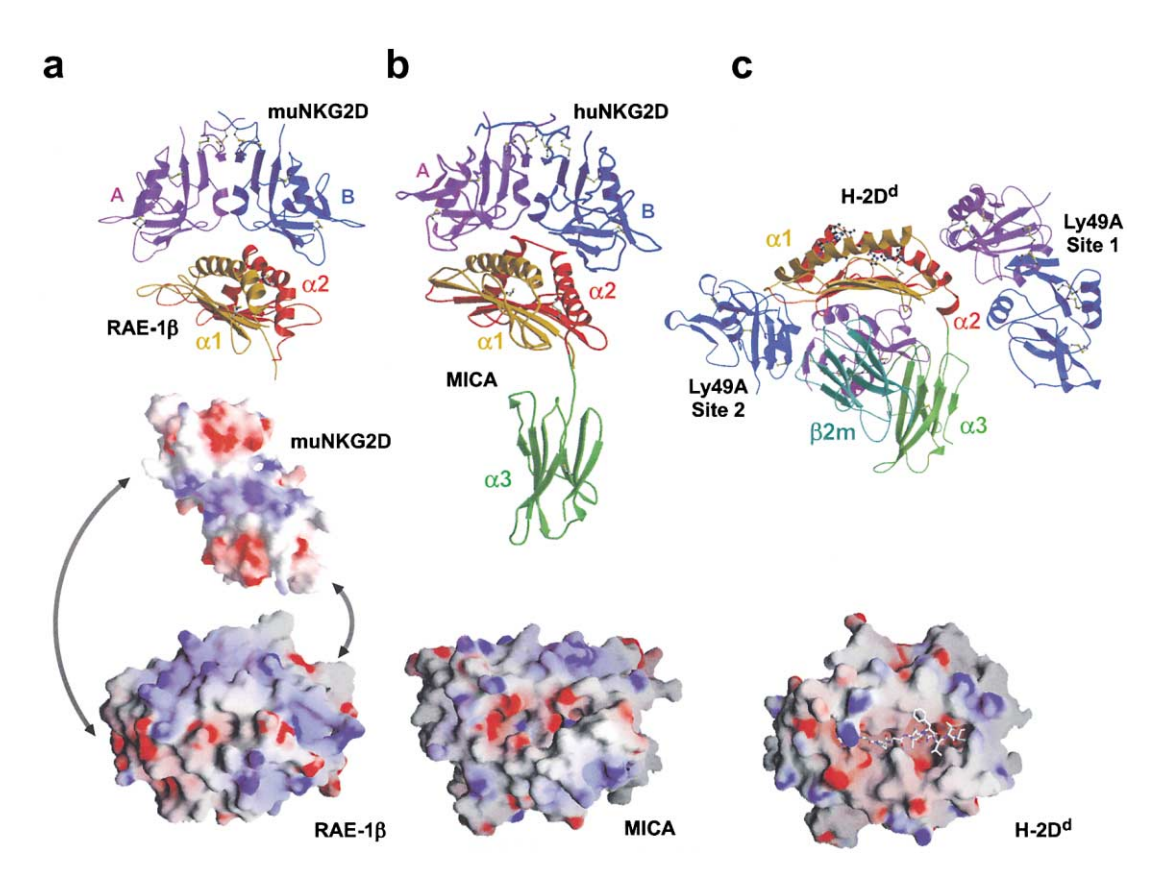


Figure 3. Structures of Murine NKD NK Cell Receptor-Ligand Complexes

Ribbon representations (top) and GRASP (Nicholls et al., 1991) molecular surfaces (bottom) are shown for the structures of (A) the muNKG2D-RAE-1 β , (B) huNKG2D-MICA, and (C) Ly49A-H-2D^d complexes. Ribbons of the ligands are colored by domain: α 1, yellow; α 2, red; α 3 (when present), green; and β_2 -m (when present), cyan; ribbons of the receptors are colored by chain: blue or purple. Molecular surfaces of the platform domains are oriented such that the view is looking down onto the NKG2D binding surface of RAE-1 and MICA. In (A), the molecular surface of muNKG2D was included in an orientation looking down onto the RAE-1 binding surface, as if the receptor had been peeled away from the complex. Molecular surfaces are colored by electrostatic potential, with positively charged areas in blue and negatively charged areas in red. In (C), the bound peptide in H-2D^d is shown in ball-and-stick representation.

	5.5.40				
muNKG2D-A	RAE-1β	RAE- 1α , γ , δ	huNKG2D-A	MICA	Contact Type
		Substitutions			(MICA-huNKG2D)
Ligand contact re	esidues common to	muNKG2D-A and -B			
Ser167	Gln70	_	Ser151	No contact	
Tyr168	Arg73	-	Tyr152	Arg74	H bond
Tyr168	Trp21	Δ	Tyr152	Met75	ϕ
Tyr168	Gln70	-	Tyr152	Lys71	VDW
Val198	No contact	=	lle182	His79	ϕ
Ile200	Pro14	=	Met184	Val18, Arg74, Ala78	ϕ
Pro201	No contact	=	Gln185	Val18	H bond
Lys213	Asn78	-	Lys197	Asp149	salt bridge
Tyr215	Asn74	Asp	Tyr199	His79	H bond
Tyr215	Arg73	_	Tyr199	Met75	ϕ
Asn223	No contact	-	Asn207	Arg38	H bond
Ligand contact re	esidues unique to m	uNKG2D-A		-	
Glu199	No contact	_	Glu183	Lys81	H bond
Lys202	Pro16	_	Lys186	Asp15, Ser17	H bonds
Glu217	No contact	_	Glu201	Arg74	salt bridge
Asn221	No contact	_	Thr205	Ser20	H bond
muNKG2D-B	RAE-1β	RAE-1 α, γ, δ	huNKG2D-B	MICA	Contact Type
markazo b	TIAL IP	Substitutions	HUINICED D	WIOA	(MICA-huNKG2D)
					(WIICA-HUNNG2D)
Ligand contact re	esidues common to	muNKG2D-A and -B			
Ser167	Glu148	Asp	Ser151	No contact	-
Tyr168	Lys151	Gln	Tyr152	His156	VDW
Tyr168	Phe155	Tyr	Tyr152	Ala159	ϕ
Val198	No contact	=	lle182	Ala162, Gln166	ϕ
Ile200	His158	Pro	Met184	His158, Ala162	ϕ
Pro201	No contact	=	Gln185	His158	H bond
Lys213	Glu159	Gly	Lys197	Asp65	salt bridge
Tyr215	Glu159	Gly	Tyr199	Asp163	H bond
Tyr215	Phe155	Tyr	Tyr199	Ala159	ϕ
Ligand contact re	esidues unique to m	uNKG2D-B			
Lys166	Glu148	Asp	Lys150	Ala150	H bond
Leu197	No contact	-	lle181	Gln166	H bond
Val207	No contact	_	Leu191	Thr155	φ
Ser211	No contact	_	Ser195	Arg64	H bond
Glu217	Lys151	Gln	Glu201	No contact	-
Asn223	Lys151	Gln	Asn207	Thr155	H bond

For comparison, the nature of the contacts in the MICA-huNKG2D complex (ϕ , hydrophobic interactions; VDW, van der Waals contacts) are listed. Residues deleted (Δ) between RAE-1 sequences are indicated. Possible salt bridges between muNKG2D and RAE-1 β are shown underlined.

total buried surface area at this interface was approximately 940 Å², a size consistent with crystal contacts but smallish for a relevant protein-protein interaction. The chance of finding a nonspecific interface burying more than this area is quite high, approximately 11% (Janin, 1997), suggesting that this complex merely represents an artifact of crystallization. However, glycosylation of Asn179 (a site conserved in huNKG2D) would not block the interaction and might actually contribute to it through potential favorable protein-carbohydrate contacts, though the surface involved on NKG2D (residues in the α 1 helix, the loop between the α 1 and 3₁₀ helices, the $\beta4$ strand, and the $\beta4\beta5'$ loop) has not been previously associated with any known or proposed carbohydrate binding site on NKDs or true C-type lectins. Therefore, because this complex was topologically compatible with a cell-cell interaction, it cannot be excluded from some physiological role, such as mediating signaling through a supramolecular complex or increasing the avidity of the interaction.

Discussion

The MICA-huNKG2D interface was significantly larger and more shape-complementary than the RAE-1βmuNKG2D interface, though consisting of a similar mixture of hydrophobic, polar, and ionic interactions. Comparisons of the structures of muNKG2D and RAE-1ß in isolation or in complex showed that both molecules bind essentially as rigid bodies, with little induced conformational change. In contrast, MICA undergoes a dramatic ordering of a loop concurrent with binding (Li et al., 2001). The binding of muNKG2D to RAE-1β was characterized by relatively fast association and dissociation rates ($k_{on} = 8.2 \times 10^5 \text{ M}^{-1}\text{s}^{-1}$; $k_{off} = 0.31 \text{ s}^{-1}$) (O'Callaghan et al., 2001), while the corresponding rates for the binding of huNKG2D to MICA were much slower ($k_{on} = 4-7 \times$ $10^4 \ M^{-1} s^{-1}; \ k_{off} = 0.04 \ s^{-1})$ (Li et al., 2001). The slower k_{on} and k_{off} rates for the MICA-huNKG2D interaction may reflect higher activation energies required to reach the transition state than for RAE-1-muNKG2D binding, a

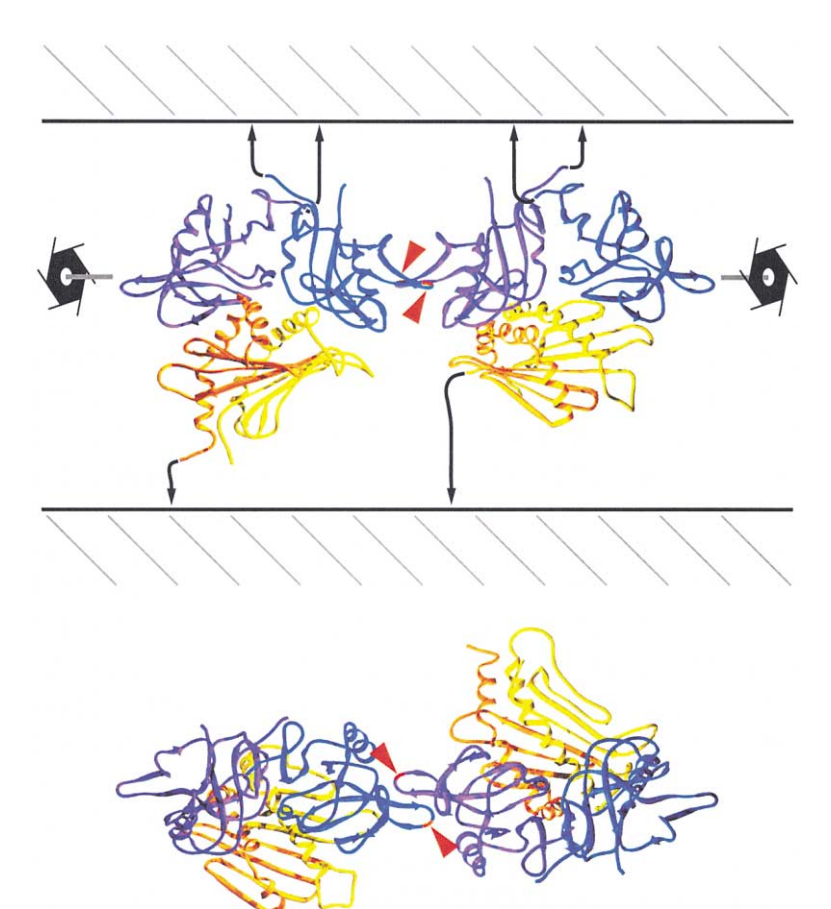


Figure 4. Interactions of RAE-1β-muNKG2D Complexes in the Crystal

Two views of the reciprocal, crystallographic interaction between muNKG2D homodimers are shown, a view perpendicular to a hypothetical cell-cell interface (top) and a view down onto the complexes (bottom). Molecules are shown as ribbon representations colored by domain (muNKG2D-A, blue; muNKG2D-B, purple; RAE-1 β α 1, yellow; and RAE-1 β α 2, orange). The approximate position of the crystallographic 6, screw axis is indicated, as are hypothetical cell surfaces and the paths of membrane anchor elements (black arrows). The position of Asn179 is indicated in red on the ribbons and by red arrows.

feature which may be explained by energetically costly conformational adjustments at the interacting surfaces during MICA-huNKG2D binding and dissociation. Although the sequences of RAE-1 isoforms are highly conserved (more than 92% identical) (Cerwenka et al., 2000), a number of substitutions in residues involved in the RAE-1 β -NKG2D interaction would be predicted to affect affinity: deletion of Trp21, His158 to Pro, and Glu159 to Gly.

There were five potential N-linked glycosylation sites in RAE-1: Asn8, Asn40, Asn53, Asn113, and Asn126. Asn8 and Asn113 were on the underside of platform domain; Asn40 and Asn126 were located in loops connecting β strands ($\beta 3\beta 4$ and $\beta 7\beta 8$); and Asn53 was at the N terminus of the $\alpha 1$ domain helix. The three potential N-linked glycosylation sites in muNKG2D were located either at the ends of the α helix (Asn137 and Asn147) or in a projecting loop (Asn179 in the $\beta 3\beta 4$ loop). All of these sites were distant from the binding surfaces, so glycosylation of either RAE-1 or muNKG2D would not be predicted to affect the affinity, consistent with published binding studies (O'Callaghan et al., 2001).

RAE-1 isoforms do not associate with β_2 -microglobulin (β_2 -m), unlike most MHC class I proteins and homologs where it is required for proper folding, with the exceptions of MICA and Zn- α_2 -glycoprotein (ZAG). An isolated platform domain of an MHC class I molecule has been shown to retain an association with β_2 -m (Collins et al., 1995). Two of the conserved N-linked glycosylation sites in RAE-1 (Asn8 and Asn113 in RAE-1 β) would, if

utilized, block the RAE-1 surface corresponding to the $\beta_2\text{-m}$ interface in $\beta_2\text{-m}$ binding MHC class I proteins. A similar situation was found in MICA (Li et al., 1999). Size exclusion chromatography (SEC)-based binding assays showed that bacterially expressed, refolded RAE-1 β , lacking N-linked oligosaccharides, also did not associate with human $\beta_2\text{-m}$ with any appreciable affinity (data not shown). However, an inspection of the RAE-1 β structure did not reveal any obvious clashes or loss of binding interactions to account for the lack of binding in the absence of N-linked glycosylation. The requirement for association with $\beta_2\text{-m}$ for folding may be obviated by the extension of the packing of the core of the domain through the interhelical hydrophobic interface and the interhelical disulfide linkage.

Both cell staining (Diefenbach et al., 2000) and SEC binding studies (data not shown) showed that muNKG2D also bound to the huNKG2D ligand MICB, but that huNKG2D did not reciprocally bind to RAE-1 β . The explanation lay in structural differences at the NKG2D β 5' β 5 stirrup loop (muNKG2D: residues 199–204, Glu-Ile-Pro-Lys-Gly-Ser; huNKG2D: residues 183–188, Glu-Met-Gln-Lys-Gly-Asp). All of the sequence differences between muNKG2D and huNKG2D ligand contact residues occurred in this loop. The stirrup loop curled inward into the binding saddle by 4–5 Å in huNKG2D relative to muNKG2D. Met184 in huNKG2D directly clashed with RAE-1 residues in a modeled hypothetical complex, thus accounting for this observation.

Despite formally representing distinct molecules, all

of the common ligand-contacting residues of muNKG2D and huNKG2D are conserved except for the Ile/Met substitution in the stirrup loop. Hence, along with the conservation of the backbone structure (an rmsd of 1.08 Å on 235 Cαs between human and murine receptors), the muNKG2D and huNKG2D ligand binding sites are essentially equivalent. Therefore, the muNKG2D-RAE-1ß complex structure reinforced the conclusion drawn from the huNKG2D-MICA structure that a single NKG2D binding surface bound with unusual promiscuity to its ligands. NKG2D has evolved a highly conserved and relatively rigid ligand binding surface that can interact specifically with strikingly different MHC-like ligands with few recognizably conserved features. On the basis of these complex structures, it would be predicted that NKG2D interacts with ULBPs and H60 through the same surface, with the ligands in a similar orientation.

Experimental Procedures

Protein Expression Crystallization and Crystallography

Soluble forms of murine RAE-1 β (residues 1–178 plus a C-terminal six histidine purification tag) and NKG2D (residues 99–234) were expressed as inclusion bodies in BL21-CodonPlus RIL cells (Stratagene), washed, solubilized in urea, and refolded by stepwise dialysis as described previously (Steinle et al., 2001). Refolded RAE-1 β was purified by nickel affinity and SEC, and NKG2D was purified by SEC alone. Analytical SEC showed that RAE-1 β was monomeric and NKG2D was homodimeric in solution. RAE-1 β -NKG2D complexes were purified by SEC for crystallization and, in solution, were consistent with a complex of one RAE-1 monomer binding to one NKG2D homodimer.

RAE-1 β was crystallized by vapor diffusion using drops consisting of two parts of protein solution (at 30 mg/ml in 25 mM PIPES, 1mM EDTA, and 0.02% NaN₃ [pH 7.0; PEA buffer]) plus one part of precipitant solution (30% w/w polyethylene glycol [PEG; M_r = 400], 0.375 M (NH₄)₂SO₄, 100 mM acetate [pH 4.5]) equilibrated over wells containing precipitant solution. RAE-1 \(\beta \) crystallized in the tetragonal space group I4₁22 with cell dimensions of a = b = 138.4 Å and c = 337.6 Å with five molecules in the asymmetric unit ($V_M = 3.9 \text{ Å}^3/\text{Da.}$). The RAE-1β-NKG2D complex was crystallized by vapor diffusion in drops consisting of one part of protein solution (at 10 mg/ml in PEA) plus one part precipitant solution (30% w/w PEG [M_r = 8000], 0.2M (NH₄)₂SO₄, and 100 mM cacodylate [pH 6.5]). The complex crystallized in the hexagonal space group P61 with lattice constants of a = b = 58.47 Å and c = 349.8 Å. The asymmetric unit contains one RAE- $1\beta\text{-NKG2D}$ complex (V $_\text{M}=$ 3.4 ų/Da). Both RAE-1 β and complex crystals were cryopreserved directly from mother liquor by dunking into liquid nitrogen. The native diffraction data sets for RAE-1 $\!\beta$ and the complex were collected at beamline 5.0.2 at the Advanced Light Source (Lawrence Berkeley National Laboratory) using a Quantum-4 CCD detector. All derivative data were collected with a Rigaku R-AXIS IV detector on an RU-200 rotating anode generator with Franks-type focusing optics (Molecular Structure Corporation). Diffraction data were processed with HKL (Otwinowski and Minor, 1997) (Table 1).

The structure of RAE-1 β was determined by MIR using one gold and two mercury derivatives (Table 1). The locations of the heavy atoms in the mercury derivatives were determined by automatic Patterson search as implemented in CNS (Brünger et al., 1998). Five heavy atom sites were found, bound specifically to the free cysteine residues (Cys69) of the five molecules in the asymmetric unit. The phases from the mercury derivatives were then used to locate the gold sites by difference Fourier syntheses. Heavy atom parameters were refined, and initial experimental phases were calculated using MLPHARE (CCP4, 1994). After density modification and phase extension in DM (CCP4, 1994), the electron density map allowed manual positioning of the platform domain of MICA for determining the averaging matrix and molecular envelope. The experimental phases were dramatically improved by subsequent 5-fold noncrystallographic symmetry averaging with DM. The initial model was built with O (Jones and Kjeldgaard, 1997) and refined in CNS against all F>0. Tight NCS restraints were applied in the early stages of refinement and gradually released in the later stages of refinement. In the final stages of refinement, after the $R_{\mbox{\scriptsize cryst}}$ dropped below 30%, NCS restraints were released and the five molecules were rebuilt separately. RAE-1 β coordinates have been deposited in the Protein Data Bank (PDB) (Berman et al., 2000), accession code 1JFM.

The structure of RAE-18-NKG2D complex was determined by molecular replacement using the refined structure of RAE-1 β and the previously published muNKG2D structure (Wolan et al., 2001) (PDB accession code 1HQ8) as search models (Table 1). NKG2D was positioned in the unit cell with AMoRe (CCP4, 1994), while the location of RAE-18 was determined with another program, MOLREP (CCP4, 1994), because AMoRe failed to give a correct solution even after a large number of trials. The correlation coefficient for the correct solution was 0.65, and the R_{cryst} was 38.8% for all data between 15 and 4.0 Å. After rigid body refinement in CNS (treating the two chains of NKG2D and RAE-1 as three separate entities) the R_{crvst} dropped to 36.3% for all reflections to 3.5 Å. The model was rebuilt against the 3.5 Å resolution electron density map to avoid close contacts between residues at the RAE-1 β -NKG2D interface and further optimized by 20 rounds of positional refinement in CNS. The R_{free} and R_{cryst} dropped to 33.0% and 31.4%, respectively, after positional and grouped B factor refinement. No further refinement was performed because of the limited resolution and quality of the diffraction data.

Acknowledgments

We thank Alexander Steinle and Thomas Spies for supplying reagents and much helpful input and Benjamin Willcox for critical comments and useful suggestions. Supported by National Institutes of Health grant Al48675 and the Pendleton Fund (to R.K.S.).

Received September 4, 2001; revised November 1, 2001.

References

Bahram, S., and Spies, T.A. (1996). Nucleotide sequence of a human MHC class I *MICB* cDNA. Immunogenetics *43*, 230–233.

Bahram, S., Bresnahan, M., Geraghty, D.E., and Spies, T.A. (1994). A second lineage of mammalian major histocompatibility complex class I genes. Proc. Natl. Acad. Sci. USA 91, 6259–6263.

Bakker, A.B., Wu, J., Phillips, J.H., and Lanier, L.L. (2000). NK cell activation: distinct stimulatory pathways counterbalancing inhibitory signals. Hum. Immunol. 61, 18–27.

Bauer, S., Groh, V., Wu, J., Steinle, A., Phillips, J.H., Lanier, L.L., and Spies, T. (1999). Activation of NK cells and T cells by NKG2D, a receptor for stress-inducible MICA. Science 285, 727–729.

Berman, H.M., Westbrook, J., Feng, Z., Gilliland, G., Bhat, T.N., Weissig, H., Shindyalov, I.N., and Bourne, P.E. (2000). The Protein Data Bank. Nucleic Acids Res. 28, 235–242.

Brünger, A.T. (1992). Free R value: a novel statistical quantity for assessing the accuracy of crystal structures. Nature 355, 472–475.

Brünger, A.T., Adams, P.D., Marius Clore, G., DeLano, W.L., Gros, P., Grosse-Kunstleve, R.W., Jiang, J.-S., Kuszewski, J., Nilges, M., Pannu, N.S., et al. (1998). Crystallography & NMR system: a new software suite for macromolecular structure determination. Acta Crystallogr. *D54*, 905–921.

Burmeister, W.P., Gastinel, L.N., Simister, N.E., Blum, M.L., and Bjorkman, P.J. (1994). Crystal structure at 2.2 Å resolution of the MHC-related neonatal Fc receptor. Nature *372*, 336–343.

CCP4 (Collaborative Computational Project 4) (1994). The CCP4 suite: programs for protein crystallography. Acta Crystallogr. D 50, 760–763

Cerwenka, A., Bakker, A.B., McClanahan, T., Wagner, J., Wu, J., Phillips, J.H., and Lanier, L.L. (2000). Retinoic acid early inducible genes define a ligand family for the activating NKG2D receptor in mice. Immunity 12, 721–727.

Collins, E.J., Garboczi, D.N., Karpusas, M.N., and Wiley, D.C. (1995). The three-dimensional structure of a class I major histocompatibility complex molecule missing the alpha 3 domain of the heavy chain. Proc. Natl. Acad. Sci. USA 92, 1218–1221.

Cosman, D., Mullberg, J., Sutherland, C.L., Chin, W., Armitage, R., Fanslow, W., Kubin, M., and Chalupny, N.J. (2001). ULBPs, novel MHC class I-related molecules, bind to CMV glycoprotein UL16 and stimulate NK cytotoxicity through the NKG2D receptor. Immunity 14, 123–133.

Diefenbach, A., Jamieson, A.M., Liu, S.D., Shastri, N., and Raulet, D.H. (2000). Ligands for the murine NKG2D receptor: expression by tumor cells and activation of NK cells and macrophages. Nat. Immun. 1, 119–126.

Diefenbach, A., Jensen, E.R., Jamieson, A.M., and Raulet, D.H. (2001). Rae1 and H60 ligands of the NKG2D receptor stimulate tumour immunity. Nature *413*, 165–171.

Esnouf, R.M. (1999). Further additions to MolScript version 1.4, including reading and contouring of electron-density maps. Acta Crystallogr. D 55, 938–940.

Groh, V., Bahram, S., Bauer, S., Herman, A., Beauchamp, M., and Spies, T. (1996). Cell stress-regulated human major histocompatibility complex class I gene expressed in gastrointestinal epithelium. Proc. Natl. Acad. Sci. USA 93, 12445–12450.

Groh, V., Steinle, A., Bauer, S., and Spies, T. (1998). Recognition of stress-induced MHC molecules by intestinal epithelial $\gamma\delta$ T cells. Science 279, 1737–1740.

Groh, V., Rhinehart, R., Secrist, H., Bauer, S., Grabstein, K.H., and Spies, T. (1999). Broad tumor-associated expression and recognition by tumor-derived gamma delta T cells of MICA and MICB. Proc. Natl. Acad. Sci. USA 96, 6879–6884.

Janin, J. (1997). Specific versus non-specific contacts in protein crystals. Nat. Struct. Biol. 4, 973–974.

Jones, T.A., and Kjeldgaard, M. (1997). Electron density map interpretation. Methods Enzymol. 277, 173–208.

Lanier, L.L. (2000). Turning on natural killer cells. J. Exp. Med. 191, 1259–1262.

Lanier, L.L., Corliss, B.C., Wu, J., Leong, C., and Phillips, J.H. (1998). Immunoreceptor DAP12 bearing a tyrosine-based activation motif is involved in activating NK cells. Nature 391, 703–707.

Laskowski, R.A., MacArthur, M.W., Hutchinson, E.G., and Thornton, J.M. (1992). PROCHECK: a program to check the stereochemical quality of protein structures. J. Appl. Crystallogr. 26, 283–291.

Lawrence, M., and Colman, P.M. (1993). Shape complementarity at protein/protein interfaces. J. Mol. Biol. 234, 946–950.

Lebrón, J.A., Bennett, M.J., Vaughn, D.E., Chirino, A.J., Snow, P.M., Mintier, G.A., Feder, J.N., and Bjorkman, P.J. (1998). Crystal structure of the hemochromatosis protein HFE and characterization of its interaction with transferrin receptor. Cell 93, 111–123.

Li, P., Willie, S.T., Bauer, S., Morris, D.L., Spies, T., and Strong, R.K. (1999). Crystal structure of the MHC class I homolog MIC-A, a $\gamma\delta$ T cell ligand. Immunity *10*, 577–584.

Li, P., Morris, D.L., Willcox, B.E., Steinle, A., Spies, T., and Strong, R.K. (2001). Complex structure of the activating immunoreceptor NKG2D and its MHC class I-like ligand MICA. Nat. Immun. 2, 443–451.

Malarkannan, S., Shih, P.P., Eden, P.A., Horng, T., Zuberi, A.R., Christianson, G., Roopenian, D., and Shastri, N. (1998). The molecular and functional characterization of a dominant minor H antigen, H60. J. Immunol. *161*, 3501–3509.

Malarkannan, S., Horng, T., Eden, P., Gonzalez, F., Shih, P., Brouwenstijn, N., Klinge, H., Christianson, G., Roopenian, D., and Shastri, N. (2000). Differences that matter: major cytotoxic T cell-stimulating minor histocompatibility antigens. Immunity *13*, 333–344.

Merritt, E.A., and Bacon, D.J. (1997). Raster3D: photorealistic molecular images. Methods Enzymol. 277, 505–524.

Nicholls, A., Sharp, K.A., and Honig, B. (1991). Protein folding and association: insights from the interfacial and thermodynamic properties of hydrocarbons. Proteins 11, 281–296.

Nomura, M., Takihara, Y., and Shimada, K. (1994). Isolation and characterization of retinoic acid-inducible cDNA clones in F9 cells: one of the early inducible clones encodes a novel protein sharing

several highly homologous regions with a Drosophila polyhomeotic protein. Differentiation *57*, 39–50.

Nomura, M., Zou, Z., Joh, T., Takihara, Y., Matsuda, Y., and Shimada, K. (1996). Genomic structures and characterization of Rae1 family members encoding GPI-anchored cell surface proteins and expressed predominantly in embryonic mouse brain. J. Biochem. (Tokyo) 120, 987–995.

O'Callaghan, C.A., Cerwenka, A., Willcox, B.E., Lanier, L.L., and Bjorkman, P.J. (2001). Molecular competition for NKG2D: H60 and RAE1 compete unequally for NKG2D with dominance of H60. Immunity 15, 201–211.

Otwinowski, Z., and Minor, W. (1997). Processing of X-ray diffraction data collected in oscillation mode. Methods Enzymol. *276*, 307–327. Sanchez, L.M., Chirino, A.J., and Bjorkman, P.J. (1999). Crystal structure of human ZAG, a fat-depleting factor related to MHC molecules. Science *283*, 1914–1919.

Steinle, A., Li, P., Morris, D.L., Groh, V., Lanier, L.L., Strong, R.K., and Spies, T. (2001). Interactions of human NKG2D with its ligands MICA, MICB, and homologs of the mouse RAE-1 protein family. Immunogenetics *53*, 279–287.

Tormo, J., Natarajan, K., Margulies, D.H., and Mariuzza, R.A. (1999). Crystal structure of a lectin-like natural killer cell receptor bound to its MHC class I ligand. Nature *402*, 623–631.

Trinchieri, G. (1989). Biology of natural killer cells. Adv. Immunol. 47, 187-376.

Weis, W.I., Taylor, M.E., and Drickamer, K. (1998). The C-type lectin superfamily in the immune system. Immunol. Rev. 163, 19–34.

Wilson, I.A., and Garcia, K.C. (1997). T-cell receptor structure and TCR complexes. Curr. Opin. Struct. Biol. 7, 839–848.

Wingren, C., Crowley, M.P., Degano, M., Chien, Y.-H., and Wilson, I.A. (2000). Crystal structure of a $\gamma\delta$ T cell receptor ligand T22: a truncated MHC-like fold. Science 287, 310–314.

Wolan, D.W., Teyton, L., Rudolph, M.G., Villmow, B., Bauer, S., Busch, D.H., and Wilson, I.A. (2001). Crystal structure of the murine NK cell-activating receptor at 1.95 Å. Nat. Immun. 2, 248–254.

Wu, J., Song, Y., Bakker, A.B., Bauer, S., Spies, T., Lanier, L.L., and Phillips, J.H. (1999). An activating immunoreceptor complex formed by NKG2D and DAP10. Science 285, 730–732.

Wu, J., Cherwinski, H., Spies, T., Phillips, J.H., and Lanier, L.L. (2000). DAP10 and DAP12 form distinct, but functionally cooperative, receptor complexes in Natural Killer cells. J. Exp. Med. 192, 1059–

Zeng, Z.-H., Castaño, A.R., Segelke, B.W., Stura, E.A., Peterson, P.A., and Wilson, I.A. (1997). Crystal structure of mouse CD1: an MHC-like fold with a large hydrophobic binding groove. Science 277, 339–345.

Zou, Z., Nomura, M., Takihara, Y., Yasunaga, T., and Shimada, K. (1996). Isolation and characterization of retinoic acid-inducible cDNA clones in F9 cells: a novel cDNA family encodes cell surface proteins sharing partial homology with MHC class I molecules. J. Biochem. (Tokyo) 119, 319–328.

Accession Numbers

RAE-1 β coordinates have been deposited in the Protein Data Bank under accession code 1JFM. Coordinates for the partially refined RAE-1 β -NKG2D complex structure have been deposited in the Protein Data Bank under accession code 1JSK.